metals

Article

Structural Optimization, Fabrication, and Corrosion Behaviors of Biodegradable Mg-Nd-Zn-Zr Alloy Hemostatic Clip

Lin Mao [1,*], Xin Zheng [1], Yongji Tian [1], Yiling Shi [1], Xiaochen Zhang [2] and Chengli Song [1,*]

[1] School of Health Science and Engineering, University of Shanghai for Science and Technology, Shanghai 200093, China
[2] College of Materials Chemical and Engineering, Heilongjiang Institute of Technology, Harbin 150050, China
* Correspondence: linmao@usst.edu.cn (L.M.); csong@usst.edu.cn (C.S.)

Abstract: In this study, the process of ligating blood vessels via biodegradable Mg alloy hemostatic clips with toothless, transverse teeth, and embedded teeth was simulated through finite element analysis (FEA). The results showed that the transverse tooth clip caused the minimum stress (0.81489 MPa) to blood vessels. Furthermore, the effects of clips with transverse teeth of different parameters, including lower tooth length, tooth height, and tooth pitch, on clamped blood vessels were studied. The numerical simulation results showed that the three optimal parameters for clips with transverse teeth were 0.2, 0.1, and 0.1 mm, respectively. Then, the optimally designed clip based on the Mg–Nd–Zn–Zr alloy was manufactured and evaluated using immersion tests. Results from the corrosion behavior study showed that closed clips (0.118 ± 0.041 mg$\cdot$cm$^{-2}\cdot$day^{-1}) corroded slightly faster than open clips (0.094 ± 0.041 mg$\cdot$cm$^{-2}\cdot$day^{-1}). Moreover, micromorphological observations showed that no cracks appeared on the closed clips, indicating that the Mg alloy had excellent performance and avoided stress corrosion cracking (SCC). Thus, the new type of Mg alloy clip kept good blood vessel closure during FEA and exhibited no corrosion cracking during the degradation process, making it a promising candidate for applications with biodegradable hemostatic clips.

Keywords: biodegradable Mg alloy; hemostatic clip; finite element analysis; structural design; corrosion behavior

Citation: Mao, L.; Zheng, X.; Tian, Y.; Shi, Y.; Zhang, X.; Song, C. Structural Optimization, Fabrication, and Corrosion Behaviors of Biodegradable Mg-Nd-Zn-Zr Alloy Hemostatic Clip. *Metals* **2022**, *12*, 1979. https://doi.org/10.3390/met12111979

Academic Editors: Kenta Yamanaka and Frank Czerwinski

Received: 30 September 2022
Accepted: 17 November 2022
Published: 19 November 2022

1. Introduction

Hemostatic clips are commonly used in laparoscopic surgery to achieve adequate hemostasis, and they can also be used as radiopaque markers and fixation tools when closing perforations and fistulas [1,2]. At present, hemostatic clips made of pure titanium (Ti) or its alloys are most regularly employed in abdominal surgery due to their high strength and excellent biocompatibility, which ensure complete occlusion of blood vessels [3]. However, Ti clips that remain in the body permanently may cause long-term adverse reactions, requiring a second surgical intervention to remove them [4]. In addition, Ti alloys can lead to artifacts in computed tomography (CT) or magnetic resonance imaging (MRI), making diagnosis of the operation area difficult [5]. Moreover, it has been reported that Ti alloys can cause allergic reactions in some patients [6,7].

In order to eliminate the disadvantages of permanent clips, hemostatic clips can be degraded and absorbed in the human body after completing their hemostatic function [8]. In the 1990s, absorbable polymeric hemostatic clips were developed, with Lapro-clips being typical representatives, that could successfully ligate tissue during appendectomies without causing postoperative complications such as bleeding or wound infection [9]. However, due to the low elasticity modulus and strength of the material, the size of the absorbable polymer clips was enlarged to meet mechanical property requirements. Moreover, absorbable polymer clips are expensive, which is challenging for ordinary people. These drawbacks have limited the widespread application of absorbable polymeric clips.

Currently, magnesium (Mg) and its alloys have emerged as important metallic implant materials due to their excellent biocompatibility and biodegradability [10–12]. Mg is an essential element for the human body and plays an important role in normal metabolic processes [13]. Excess Mg cations can be absorbed by the surrounding tissues or excreted through urine in the human physiological environment without causing toxicity [14]. In addition, the density and Young's modulus of Mg alloys are similar to those of human bone, enabling Mg-based orthopedic implants to reduce the stress shielding effect [15]. To date, Mg alloys have been extensively studied in orthopedic implants [16], cardiovascular stents [17,18], and tissue engineering scaffolds [19]. Unfortunately, rapid degradation of Mg alloys may result in deterioration of the mechanical properties of the implants before tissues have completely healed, which hinders their clinical application as load-bearing implant devices [13,20]. Meanwhile, rapid corrosion of Mg alloys accompanied with the evolution of large amounts of hydrogen gas can lead to the formation of gas cavities, and a shift to alkaline conditions surrounding the implants may cause adverse effects, such as tissue inflammation or alkalosis [21–23]. However, the mechanical strength of the material required for hemostatic clips only needs to be maintained for approximately two weeks; therefore, the corrosion resistance of Mg alloy clips is not as strict as that for orthopedic implants [3,4,8]. Several studies exploring Mg alloy hemostatic clips have been published in recent years. Ikeo et al. fabricated a biodegradable Mg-Zn-Ca hemostatic clip that successfully ligated the renal veins of rats without causing tissue inflammation around the implantation area [1]. Yu et al. developed a new Mg-Zn-Ca-Y alloy clip that successfully occluded the carotid artery of a rat with no adverse reactions after surgery [8].

In this work, Mg–Nd–Zn–Zr alloy, which exhibited uniform corrosion behavior, excellent mechanical properties, and blood compatibility in previous studies [24,25], was applied to develop a new type of biodegradable hemostatic clip. The structure of the clip was designed and optimized through finite element analysis, aiming to achieve complete occlusion of blood vessels while inducing only minor mechanical damage. Then, the optimally designed clip was fabricated using the electrical discharge wire-cutting method. Furthermore, in vitro immersion tests were used to evaluate the corrosion behavior of the Mg alloy clip, and the underlying degradation mechanism of the material was characterized to gain a better understanding of the clip corrosion process in artificial plasma.

2. Materials and Methods

2.1. Structural Design and Optimization

The structural dimensions of the designed Mg–Nd–Zn–Zr alloy hemostatic clips are shown in Figure 1 (denoted as NS, TS, and FS, respectively). It can be seen that the thickness of all the clip arms gradually increases from the tail end to the top. The circular opening at the top of the NS clip is small, which allows blood vessels to be clamped more tightly (Figure 1a). The TS clip structure has tiny transverse teeth (Figure 1b). The FS clip structure has tiny vertical teeth (Figure 1c). Figure 1d depicts the tooth profile parameters: $L2$ is the lower tooth length; $L1$ is the upper tooth length ($L2 = 2L1$); h is the tooth height; and p is the tooth pitch.

According to the results of the finite element analysis (Section 3.1), the TS clip slightly reduced the damage to blood vessels compared to the NS and FS clips. Then, the clip with transverse teeth was further optimized. Three different tooth profile parameters were chosen to modify the structural design, and the specific size parameters are shown in Table 1.

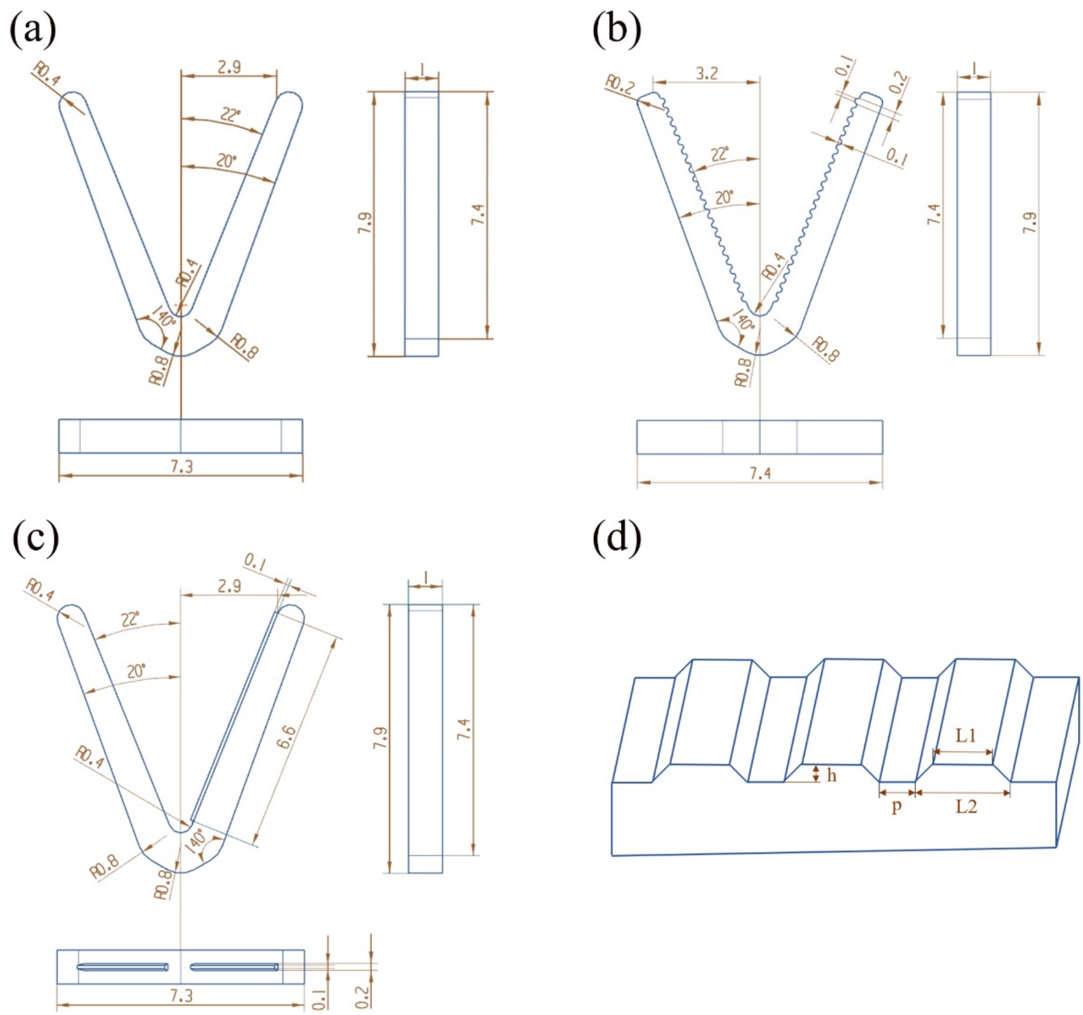

Figure 1. Structural dimensions of the designed hemostatic clips: (**a**) NS; (**b**) TS; (**c**) FS; (**d**) Schematic diagram of tooth profile parameters (mm).

Table 1. Size parameters of transverse tooth clips.

Number	Tooth Length *L1* (mm)	Tooth Length *L2* (mm)	Tooth Height *h* (mm)	Tooth Pitch *p* (mm)	Denotation
1	0.1	0.2	0.1	0.1	TS1
	0.15	0.3			TS2
	0.2	0.4			TS3
2	0.1	0.2	0.1	0.1	
			0.15		TS4
			0.2		TS5
3	0.1	0.2	0.1	0.1	
				0.2	TS6
				0.3	TS7

2.2. Finite Element Analysis of Mg Alloy Clip

The geometric models of the hemostatic clips and blood vessels were established using Unigraphics NX 10.0 software (Siemens PLM Software, Dallas, Texas, TX, USA) in this work. Mg-Nd-Zn-Zr alloy was used as the material for the hemostatic clips. The selected middle vein segment had an inner diameter of 2.5 mm, wall thickness of 0.25 mm, and length of 10 mm. The Mooney-Rivlin 5 model was used as the material for the blood vessels. Table 2 lists the specific parameters of the Mg-Nd-Zn-Zr alloy and Mooney-Rivlin

5 model. The assembled model of the Mg alloy clip and blood vessel was imported for finite element analysis in ANSYS Workbench 19.2 software (ANSYS, Canonsburg, PA, USA) and meshed. The insides of both arms of the hemostatic clip were arranged in contact with the outer surface of the blood vessel. Both ends facing the vessel segment were fully fixed. Displacement changes were applied to the two arms of the hemostatic clip. Finally, a nonlinear solution was performed in ANSYS Workbench software19.2. The stress and strain distribution of the hemostatic clip and blood vessel induced by ligating the blood vessel with the clip were obtained in the simulation.

Table 2. Material parameters of Mg-Nd-Zn-Zr alloy and Mooney-Rivlin 5 model.

Materials	Input Parameters
Mg-Nd-Zn-Zr alloy	Density = 1.8 g/cm^3 Young's modulus = 42 GPa Poisson's ratio = 0.35
Mooney-Rivlin 5 model	C10 = 1.89×10^4 Pa C01 = 2.75×10^3 Pa C20 = 8.572×10^4 Pa C11 = 5.9043×10^5 Pa C02 = 0 Pa Incompressible parameters D1 = 5×10^{-5} Pa^{-1}

2.3. Sample Preparation

The prepared as-extruded Mg–Nd–Zn–Zr alloy rods were cut into Ø12 mm × 1.2 mm sheets. The wire-cutting process was applied to cut circular sheets into the shape and size of the TS1 clip for immersion tests. The samples were ground to a thickness of 1 mm using SiC paper #7000 and then polished using a polishing agent. After ultrasonically cleaning the samples in absolute ethanol for 5 min, the clips were placed in a constant temperature drying oven for 24 h.

2.4. Microstructural Observation

The cold mounting method was used to mold the hemostatic clips for microstructural observation into epoxy resin, with only one side exposed. The samples were successively ground using SiC papers #320, #1200, #3000, and #7000 with the vertical scratch method and then cleaned with alcohol. After drying, the polished samples were etched with picric acid solution (4.2 g picric acid + 10 mL acetic acid + 10 mL distilled water + 70 mL alcohol). The corroded samples were rinsed with alcohol, followed by drying in a drying dish for 2 h. Microstructural observations were conducted using a Leica DM2700M metallographic microscope. The corrosion morphologies of the samples were observed using field emission scanning electron microscopy (FE-SEM, GeminiSEM 300, ZEISS, Baden-Wurttemberg, Germany). The element content was analyzed using energy disperse spectroscopy (EDS, AZtec X-MaxN 80, Oxford Instruments, Oxford, UK) equipped with SEM. The phase composition was analyzed using an X-ray diffractometer (XRD, Rigaku SmartLab, Rigaku, Akishima, Japan) with a standard Cu target, 40 kV working voltage, 200 mA working current, scanning range of 20°–80°, and scanning speed of 5°/min. Spectral analysis was performed using X-ray photoelectron spectroscopy (XPS, ESCALAB 250Xi, Thermo Fisher Scientific, Waltham, MA, USA).

2.5. In Vitro Corrosion Properties

In this research, in vitro immersion tests were performed in artificial plasma to study the biocorrosion behaviors of the Mg-Nd-Zn-Zr alloy clips. The components of the artificial plasma are listed in Table 3. Immersion tests of the Mg-based clips were conducted according to ASTM-G31–72. The pH value of the artificial plasma was adjusted to 7.4 with HCl before the experiments. The ratio of artificial plasma volume (mL) to the clip surface area (cm^2) was set to 1.8 mL/mm^2. The artificial plasma was kept at 37 ± 0.5 °C during the experiments, and the solution was renewed every 24 h. The pH value of the solution for each 24 h immersion of the Mg alloy clips was measured using a pH meter (SMART, Dongguan Wanchuang Electronic Products, Guangdong, China). The volume of hydrogen gas produced by degradation of the Mg alloy clips was recorded using an inverted graduated pipette. After 14 days of degradation, the samples were removed from the artificial plasma. Then, the samples were cleaned with standard CrO_3 solution, as recommended by ASTM-G1-90, to remove corrosion products formed on the surface. For the weight loss experiment, three sets of parallel samples were tested from each group, and the corrosion rate (CR) was calculated according to the following formula:

$$\mathrm{CR} = (8.76 \times 10^4 \times \mathrm{W})/(\mathrm{A} \times \mathrm{T} \times \mathrm{D}) \quad (1)$$

where W (g) is the weight change before and after immersion, A (cm^2) is surface area of the Mg-based clip exposed to artificial plasma, T (h) is the immersion time, and D (g/cm^3) is the density of the Mg-Nd-Zn-Zr alloy.

Table 3. Components of the artificial plasma (g/L).

NaCl	$CaCl_2$	KCl	$MgSO_4$	$NaHCO_3$	Na_2HPO_4	NaH_2PO_4
6.8	0.2	0.4	0.1	2.2	0.126	0.026

3. Results

3.1. Numerical Simulation Results and Analysis

Figure 2a–c show cloud images of the deformation of the hemostatic clips (NS, TS, and FS). The tip deformations of the three operative clips were all approximately 2.7 mm, and the blood vessels were fully occluded, which met the requirements of the surgery. Figure 2d shows the results of the equivalent plastic strain distribution of the TS clip after closing the vessel. The maximum plastic strain occurred at the inner arc of the top of the clip, which is the area of stress concentration. The strain cloud image of a blood vessel closed by the TS clip is shown in Figure 2e, and the maximum vascular strain was 0.28732. The largest area of vascular strain, as shown in Figure 2f, was located on the inside of the vessel wall.

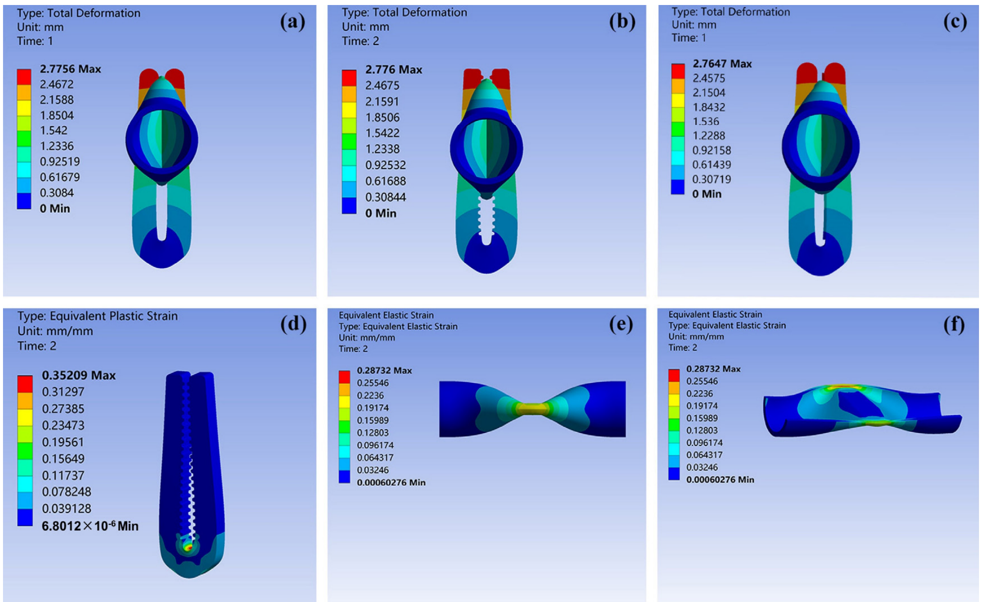

Figure 2. Finite element analysis results of hemostatic clips and blood vessels: (**a**–**c**) Deformation cloud images of the clips (NS, TS, and FS); (**d**) Equivalent plastic strain distribution cloud map of TS clip after occluding the vessel; (**e**) Strain distribution of the vessel clamped by TS clip; (**f**) Strain distribution of the vessel clamped by TS clip (cross-sectional view).

Figure 3a shows the numerical results of finite element analysis of the hemostatic NS, TS, and FS clips, in which the NS clip was used as the control group. The maximum equivalent plastic strain of the TS clip was 0.35209, which was the lowest strain among the three groups. The maximum equivalent stress (0.81489 MPa) produced by the TS clip in the blood vessel was 7.46% lower than that produced by the NS clip (0.88058 MPa) in the same vessel. The TS clip with tiny transverse teeth could prevent the blood vessel segment from being clamped too tightly, thereby reducing pressure on the vessel. In addition, the maximum equivalent stress produced by the FS clip (1.6325 MPa) in the blood vessel was 85.39% higher than that produced by the NS clip (0.88058 MPa) in the vessel. The FS clip exerted greater stress in the blood vessel because the upper and lower tooth surfaces of the embedded teeth were completely fitted, which could produce greater shear force on the clamped venous segment. The results showed that the design of the tooth shape had a significant impact on the stress distribution in the blood vessel. Moreover, the concentration of local stress in the blood vessel was inevitable after ligating the vessel with the surgical clip. However, reasonable structural design is a practical way to minimize stress in the blood vessel. Among the three preliminary designs, the TS clip was a better structure because it exerted the lowest maximum plastic strain and caused the least maximum equivalent stress to the venous segment.

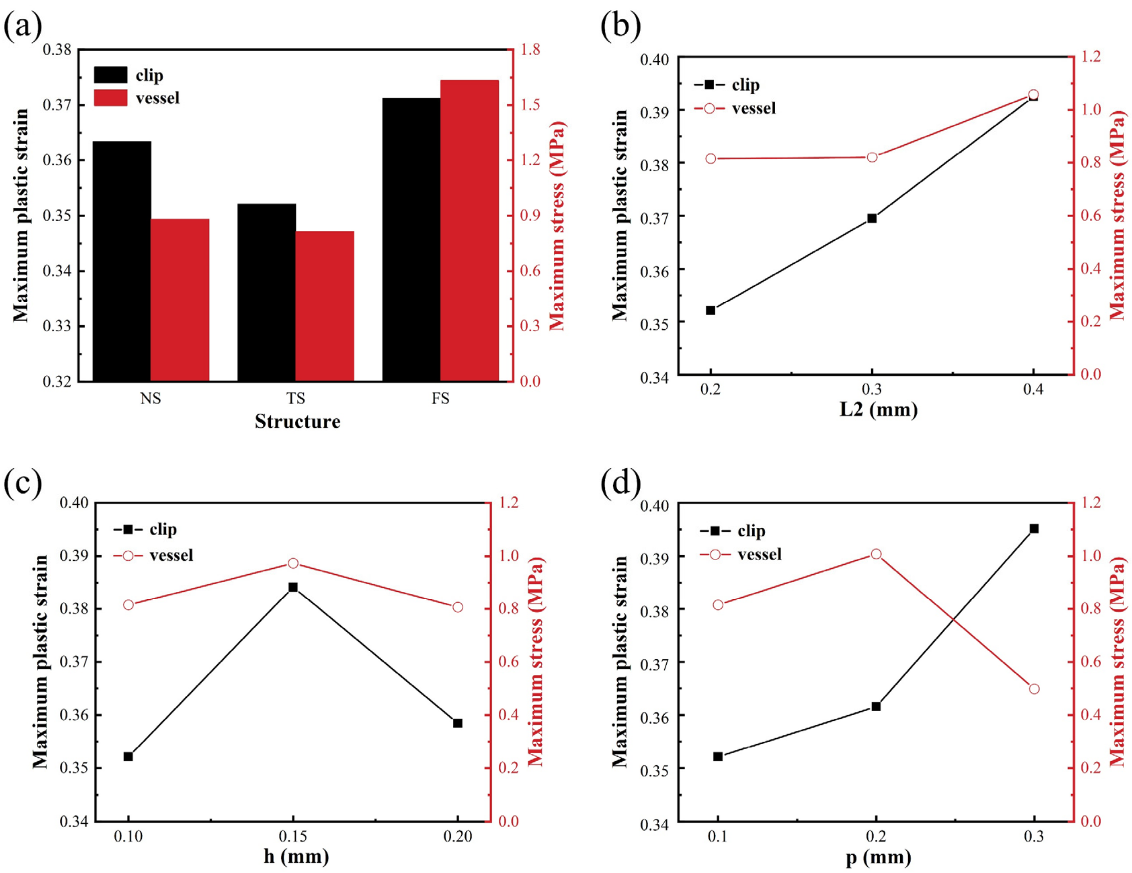

Figure 3. Numerical results of the finite element analysis of the hemostatic clips with different structural designs: (**a**) Maximum equivalent plastic strains of the Mg alloy clips and maximum equivalent stress of blood vessels; (**b**) Variation curves of the maximum equivalent plastic strain of the Mg-based clip with the lower tooth length and maximum equivalent stress of blood vessels; (**c**) Curves of the plastic strain of the clip with tooth height and maximum stress of blood vessels; (**d**) Curves of the maximum strain of the clip with tooth pitch and maximum stress of blood vessels.

The finite element analysis results of the clips (TS1, TS2, and TS3) with different tooth lengths are shown in Figure 3b. It can be seen that both the maximum plastic strain of the clips and maximum equivalent stress in blood vessels were increased with the lower tooth length. When the lower tooth length was 0.4 mm, the maximum equivalent stress produced by the TS3 clip (1.0581 MPa) in the blood vessel was 28.98% higher than that produced by the TS2 clip (0.82039 MPa) in the vessel. When the lower tooth length was 0.2 mm, the TS1 clip produced the lowest maximum equivalent stress in the blood vessel among the three groups. Consequently, the TS1 clip was the optimal design among the three clips, with *L2* and *L1* parameter values of 0.2 mm and 0.1 mm, respectively.

The finite element simulation results of the clips (TS1, TS4, and TS5) with different tooth heights are shown in Figure 3c. It can be seen that the maximum plastic strain of the Mg alloy clip increased and then decreased with increasing tooth height, which was similar to the maximum equivalent stress in the blood vessel. The stress produced by the TS1 clip in the blood vessel was close to that produced by the TS5 clip. When the tooth height was 0.1 mm, the TS1 clip produced the lowest maximum plastic strain on the hemostatic clip among the three structures, indicating that the TS1 clip was the optimal design.

The finite element simulation results of the clips (TS1, TS6, and TS7) with different tooth pitches are shown in Figure 3d. It can be seen that the maximum plastic strain of the clip was proportional to the tooth pitch. The lowest maximum plastic strain on the hemostatic clip among the three structures occurred when the tooth pitch was 0.1 mm. In addition, the maximum equivalent stress in the blood vessel increased and then decreased with increasing tooth pitch. When the tooth pitch was 0.3 mm, the TS7 clip produced the lowest maximum equivalent stress on the blood vessel among the three groups. However, the TS7 clip had the largest maximum plastic strain, which was likely to cause cracks during practical use. Considering the structural safety of the hemostatic clip and damage to blood vessels, the optimal parameter of the tooth pitch was 0.1 mm among the three clips. Finally, based on the results of the finite element analysis, the TS1 clip was considered to be the best option among all of the structural designs.

3.2. Sample Preparation and Microstructural Observations

The hemostatic clips manufactured from the Mg-Nd-Zn-Zr alloy are shown in Figure 4a. The XRD pattern of the Mg alloy is shown in Figure 4b, and the volume fraction of $Mg_{12}Nd$ calculated by MDI Jade 6 software (Materials Data, Livermore, CA, USA) was 1.2%. Table 4 lists the chemical composition of the Mg-Nd-Zn-Zr alloy. Neodymium (Nd) is non-toxic rare earth (RE) metal element, and the intermetallic phase $Mg_{12}Nd$ (Figure 4b) formed by Nd and Mg can hinder the movement of dislocations and strengthen the alloy [26]. The microalloying of Zn can improve the ductility of Mg alloys [17,27]. In aluminum-free Mg alloys, Zr is a grain refiner, which is beneficial for refining the grain size and improving the mechanical properties of Mg alloys [26,28]. The typical regions selected for optical observation are shown in Figure 5a. It is clear that the grains of the Mg-Nd-Zn-Zr alloy are fine and uniform (Figure 5b). The average grain size of the Mg alloy measured using LAMOS software was 19.49 $\pm$ 1.41 um. It is visible from the images that a few twins appeared in the stress concentration region after the Mg alloy clip was closed (Figure 5c,d), and the width of the twins was approximately 11.57 um.

Table 4. Chemical composition of the Mg-Nd-Zn-Zr alloy.

Element	Nd	Zn	Al	Zr	Mn	Mg
wt.%	2.5	0.21	-	0.44	-	Bal.

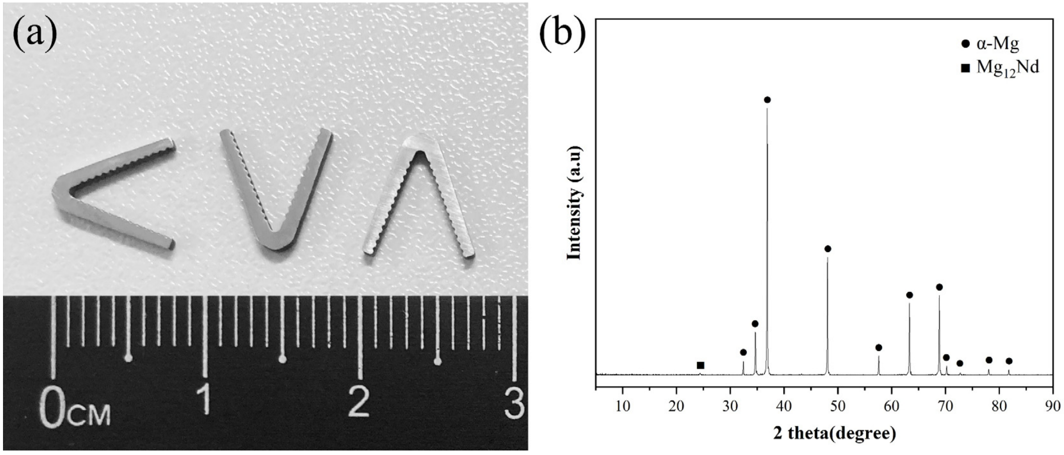

Figure 4. Mg alloy clips and the phase composition: (**a**) Image of hemostatic clips manufactured from Mg-Nd-Zn-Zr alloy; (**b**) XRD pattern of Mg-Nd-Zn-Zr alloy.

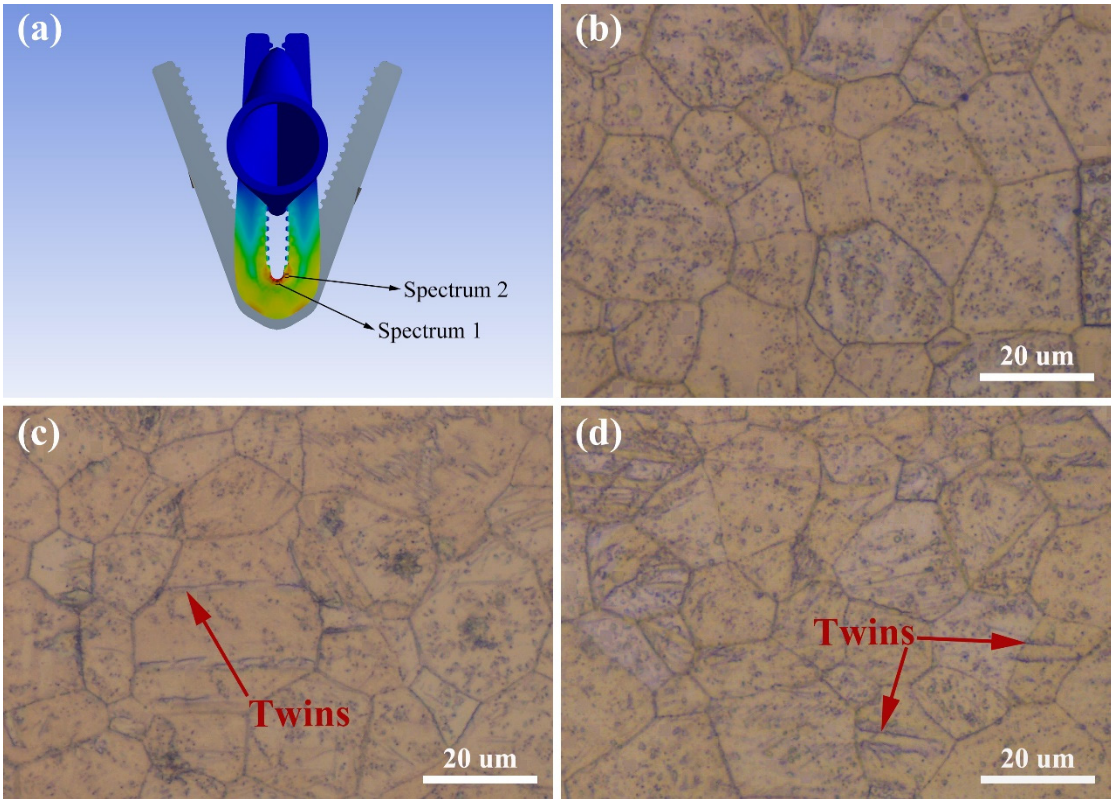

Figure 5. Microstructure of the as-extruded Mg-Nd-Zn-Zr alloy clip: (**a**) Regions for optical observation, (**b**) Typical microstructure of the Mg-Nd-Zn-Zr alloy; (**c**) Microstructure of spectrum 1 after the clip is closed; (**d**) Microstructure of spectrum 2 after the clip is closed.

3.3. In Vitro Corrosion Properties

The in vitro corrosion properties of the Mg-Nd-Zn-Zr alloy clips were investigated using immersion tests, and hydrogen (H_2) evolution and pH value were also recorded (Figure 6). The results indicated that the H_2 production volume of all clips was less than 0.3 mL/cm^2 and the H_2 production volume of the closed clip was slightly higher than that of the open clip (Figure 6a). Figure 6b shows the pH variation curves of the artificial plasma during immersion of the surgical clips. It is obvious from the results that the pH value of the artificial plasma increased sharply from 7.4 to 8.2 during the first day of degradation. After 3 days of immersion, the pH value of the solution stabilized to approximately 8.9. In addition, the pH value of the artificial plasma for the closed group was slightly higher than that for the open group from the 11th to 14th day of immersion.

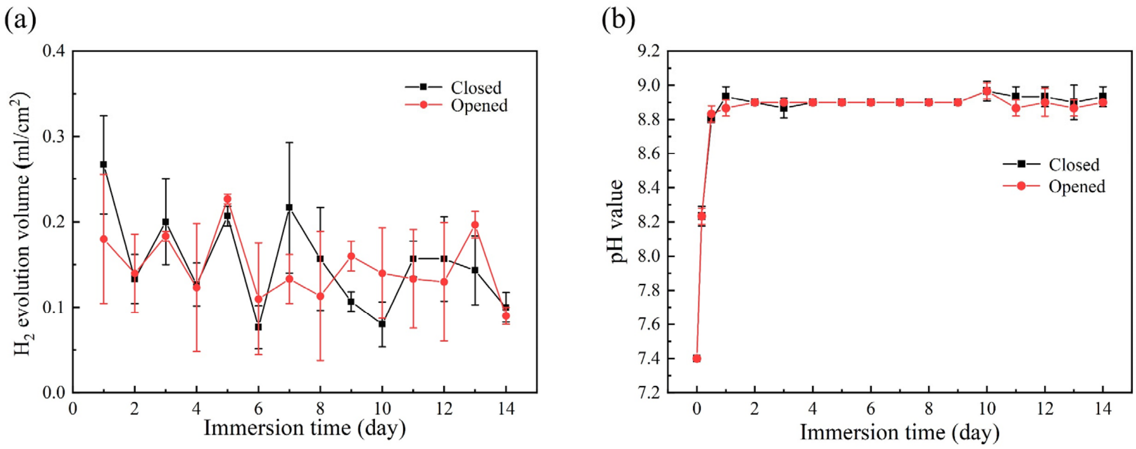

Figure 6. Immersion test of Mg-Nd-Zn-Zr alloy clips in artificial plasma for 14 days: (**a**) Volume of H_2 produced by the Mg alloy clips, (**b**) pH value variations of artificial plasma during immersion of the Mg alloy clips.

The macroscopic corrosion morphology of the closed Mg alloy clip is shown in Figure 7a, revealing that no cracks appeared on the surface of the hemostatic clip. The micro-morphologies of the Mg alloy clips were characterized by SEM (Figure 7b–f). After 14 days of degradation, a large number of corrosion products with white particles were produced on the surface of the hemostatic clip (Figure 7b,c). After cleaning the corrosion products with chromic acid solution, the morphologies of the top and tail end of the closed clip were evaluated (Figure 7d,e). The images revealed a large number of tiny corrosion pits and a few grooves on the top surface of the clip, which indicated that the corrosion behavior of the closed clip included pitting corrosion and filiform corrosion (Figure 7d). In addition, more severe corrosion was evident at the top of the clip, which is the region of plastic deformation along with stress concentration (Figure 7d,e). It is clear from the images that the distribution of corrosion pits in the open clip was relatively uniform after removing the corrosion products (Figure 7f). Research has shown that SCC may occur in Mg alloys under the combined action of electrochemistry and mechanics [29]. The corrosion morphological observations showed that no cracks appeared on the closed clip, indicating that the Mg alloy had excellent performance and avoided SCC in artificial plasma (Figure 7a,d). Then, the corrosion rate of the Mg alloy surgical clip in artificial plasma was calculated according to the results of the weight loss experiment. As shown in Figure 7g, the corrosion rate of the closed Mg alloy clip was approximately 0.118 ± 0.041 mg·cm^{-2}·day^{-1}, which was higher than that obtained for the open clip (0.094 ± 0.041 mg·cm^{-2}·day^{-1}).

According to the SEM-EDS results (Figure 8), the corrosion products on the surface of the Mg alloy hemostatic clip were composed of elements O, Ca, P, Mg, Na, Cl, and K. To further determine the chemical composition of the corrosion products, XPS surface survey scans were performed, as shown in Figure 9a–d. The full XPS spectrum showed that the corrosion products were mainly composed of elements O, Ca, Mg, Na, and P (Figure 9a), which was consistent with the results of the SEM-EDS analysis. The refined spectrum of Mg1s showed a single peak at 1303.98 eV, which corresponded to $Mg(OH)_2$ (Figure 9b). Both peaks at Ca2$p_{1/2}$ (350.78 eV) and Ca2$p_{3/2}$ (347.18 eV) corresponded to Ca^{2+} (Figure 9c). The refined spectrum of P2p showed a single peak at 133.12 eV, which corresponded to PO_4^{3-} (Figure 9d). Therefore, the composition of the corrosion product was mainly $Mg(OH)_2$ and various calcium phosphate precipitates.

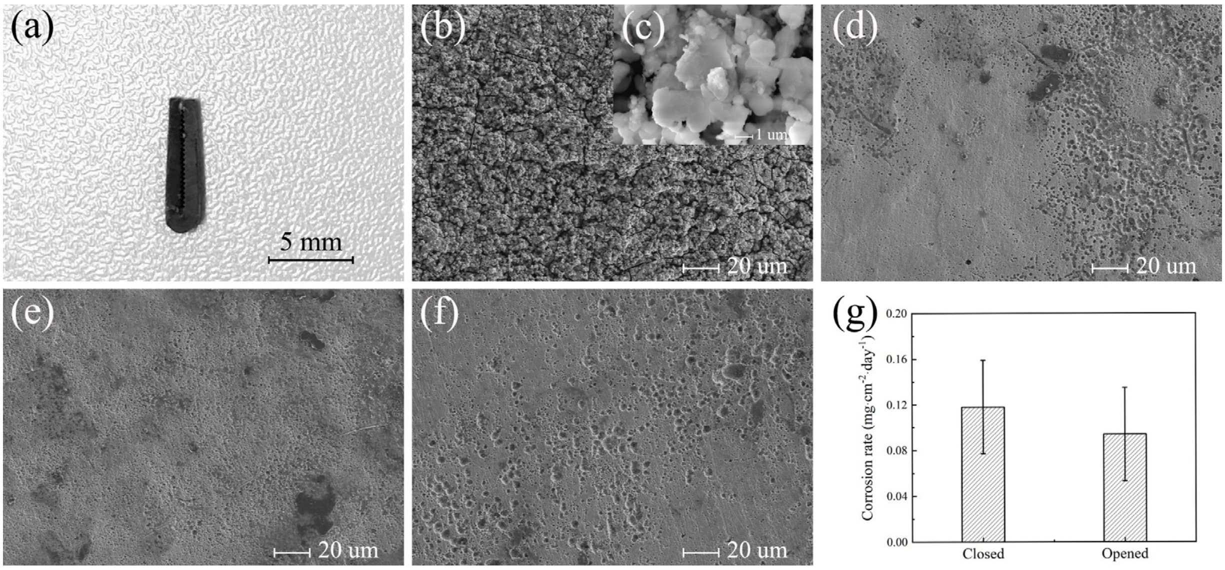

Figure 7. Corrosion behavior of Mg-Nd-Zn-Zr alloy clips in artificial plasma: (**a**) Macroscopic corrosion morphology of the closed clip; (**b**) Micromorphology of the top region of the closed clip after 14 days of immersion; (**c**) Amplified morphology of corrosion products; (**d**) Surface morphology of the top region of the closed clip after removing the corrosion products, (**e**) Surface morphology of the tail end of the closed clip after cleaning the corrosion products; (**f**) Surface morphology of the open clip after cleaning the corrosion products; (**g**) Corrosion rates of the closed and open clips achieved by weight loss calculation after degradation for 14 days.

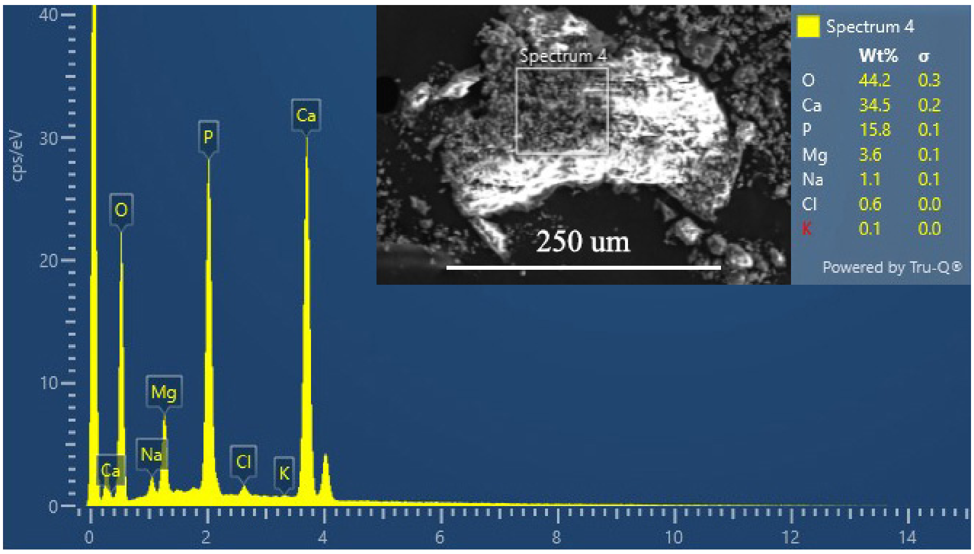

Figure 8. SEM-EDS results of the corrosion products on the surface of Mg-Nd-Zn-Zr alloy clips.

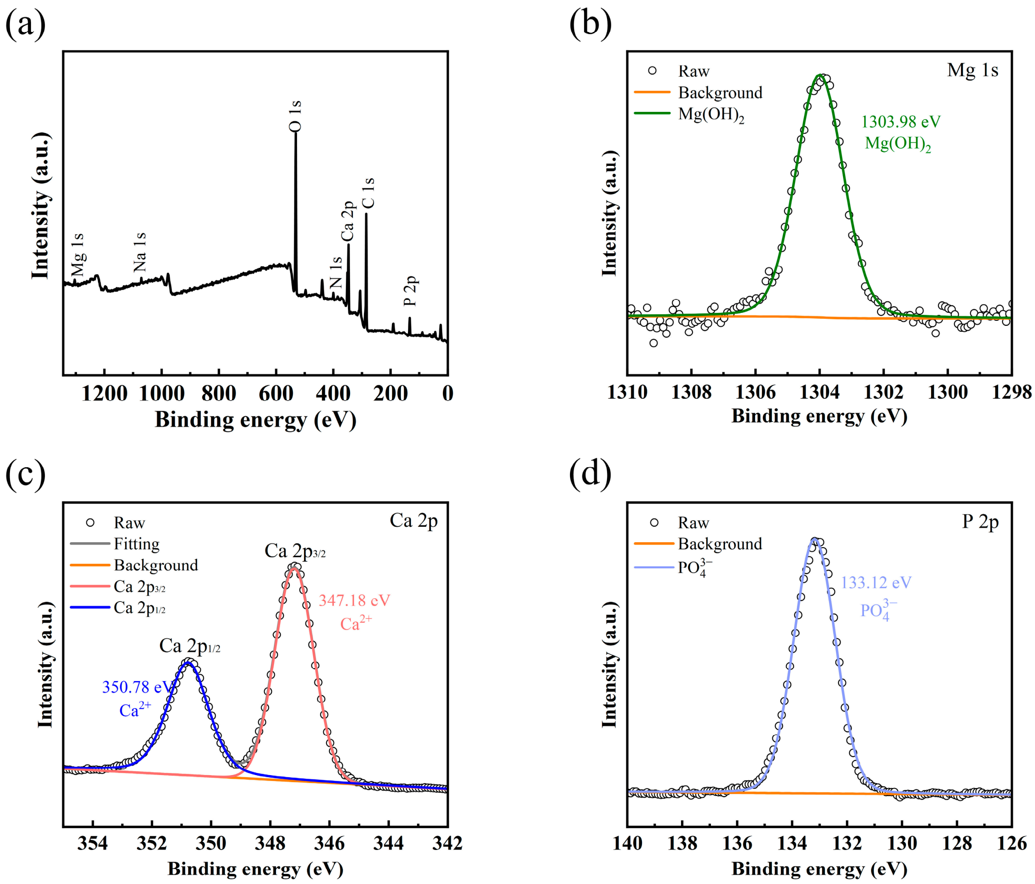

Figure 9. XPS spectra for the corrosion products on Mg alloy hemostatic clips: (**a**) XPS surface survey scan; (**b**) Mg1s; (**c**) Ca2p; (**d**) P2p.

4. Discussion

Ti and its alloys are commonly used as materials for laparoscopic hemostatic clips, but they are not biodegradable and often require a second surgery to remove them [4,16]. Although currently approved biodegradable polymers (such as PGA and PLGA) can be used in clinical implantable devices, their degradation products may cause adverse biological reactions [17,27,30]. Mg alloys appear to be revolutionary biomaterials for degradable clips as they can meet both engineering and medical needs [3,31,32]. Hemostatic clips manufactured from Mg alloys can be completely degraded in the human physiological environment. However, the application of Mg-based hemostatic clips is limited by their rapid corrosion rate, pitting corrosion, and SCC, which will lead to early failure of the implants [12,33,34].

The poor corrosion resistance of Mg alloys can be attributed to galvanic corrosion caused by the second phase and impurity elements [35]. Figure 10 illustrates the degradation mechanism of the Mg-Nd-Zn-Zr alloy clip in artificial plasma. Immediately after contact with the artificial plasma, the Mg alloy is oxidized to Mg ions (Figure 10a). Meanwhile, the generated electrons react with water to produce hydrogen (Figure 10a). Consequently, Mg ions and hydroxide ions in the solution react to form Mg hydroxide:

$$Mg \rightarrow Mg^{2+} + 2e^- \quad (\text{anodic reaction}) \tag{2}$$

$$2H_2O + 2e^- \rightarrow H_2 + 2OH^- \quad (\text{cathodic reaction}) \tag{3}$$

$$Mg^{2+} + 2OH^- \rightarrow Mg(OH)_2 \tag{4}$$

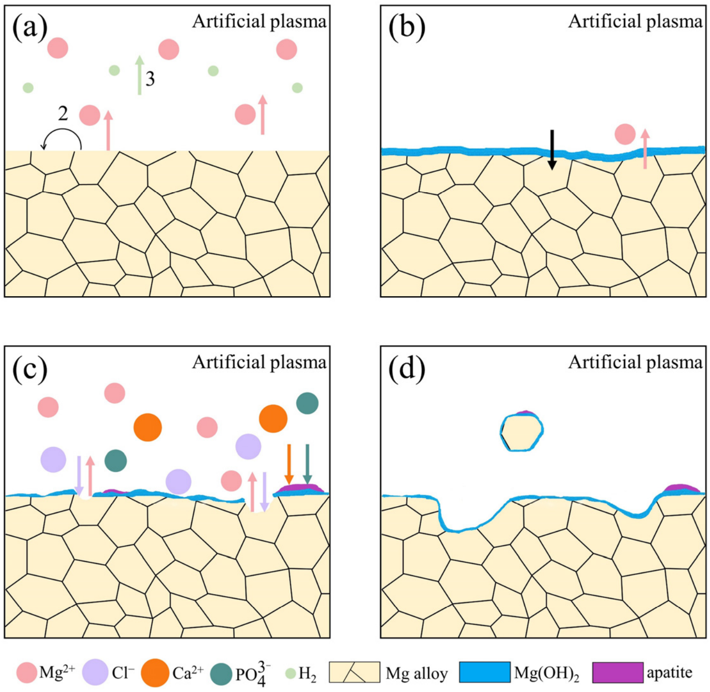

Figure 10. Schematic diagram of biocorrosion of Mg-Nd-Zn-Zr alloy clips: (**a**) Anodic reaction and cathodic reaction; (**b**) Formation of Mg hydroxide; (**c**) Chloride ions destroy the protective layer and formation of apatite; (**d**) Mg alloy is in the state of dynamic degradation.

As illustrated above, the corrosion products $Mg(OH)_2$ on the surface of the hemostatic clip can delay the degradation process of the Mg substrate (Figure 10b) [12]. However, porous Mg hydroxide on the surface cannot protect the Mg matrix effectively under erosion by Cl^-. It is reported that when the chloride concentration in the physiological environment reaches 30 mmol/L, $Mg(OH)_2$ will be gradually converted by Cl^- to form $MgCl_2$, which is easily soluble in water (Figure 10c) [33]:

$$Mg(OH)_2 + 2Cl^- \rightarrow MgCl_2 + 2OH^- \tag{5}$$

Thus, the Mg substrate is exposed for further reaction with artificial plasma (Figure 10c). According to the results of the spectral analysis (Figure 9), in addition to Mg hydroxide, the corrosion products also included various calcium phosphate precipitates, such as hydroxyapatite (HA), which is an effective barrier to delay the degradation of the corrosion layer (Figure 10c,d) [36]:

$$10Ca^{2+} + 6PO_4^{3-} + 2OH^- \rightarrow Ca_{10}(PO_4)_6(OH)_2 \tag{6}$$

The results indicated that Both the closed and open Mg alloy clips exhibited low corrosion rates in artificial plasma (Figure 7g). There are three possible reasons for this phenomenon. First, the microstructural observations revealed that the grain size of the Mg-Nd-Zn-Zr alloy was uniform and fine (Figure 5b). It is widely accepted that grain refinement can improve the corrosion resistance of Mg alloys [37]. Secondly, the second phase also has an impact on the corrosion behavior of Mg alloys [35]. The potential difference between the second phase $Mg_{12}Nd$ and the α-Mg matrix was approximately 25 mV, indicating that microgalvanic corrosion in the Mg-Nd-Zn-Zr alloy occurred at a low level [25]. Moreover, the properties of MgO films formed on the surface of the Mg alloy are related to corrosion resistance [38], and an excellent passivation film can restrain the outflow of Mg^{2+} from the substrate surface [39]. Studies have shown that the addition of element Nd can form an excellent rare earth oxide film on the surface, thereby improving the corrosion resistance of Mg alloys [40,41]. Thus, the Mg-Nd-Zn-Zr alloy clips exhibited excellent corrosion resistance in artificial plasma.

The results indicated that the corrosion rate of the closed clips was higher than that of the open clips (Figure 7g), and the microstructural characterization showed that the corrosion on the top of the closed clip was more severe than that in other regions (Figure 7d,e). This result can be attributed to the closed hemostatic clip undergoing dramatic plastic deformation, resulting in a certain number of twins in the stress concentration regions (Figure 5d). It is universally acknowledged that atoms in twin regions are more active than those in normal lattice positions [42]. In addition, the anodic dissolution of twins is accelerated compared with the Mg matrix [8]. Aung et al. reported that the existence of twins accelerated the corrosion of Mg alloys [43]. Therefore, the closed Mg-Nd-Zn-Zr alloy clip with several regions containing twins could degrade faster in artificial plasma.

5. Conclusions

Based on the results of the finite element analysis, the hemostatic clip with transverse teeth was the optimal structure for ligating veins with minor damage to blood vessels, compared to clips without teeth or with embedded teeth. The optimal parameters for lower tooth length, tooth height, and tooth pitch of the hemostatic clip with transverse teeth were 0.2, 0.1, and 0.1 mm, respectively. The optimally designed Mg-Nd-Zn-Zr alloy clip was processed using the wire-cutting method, and a few twins appeared in the stress concentration regions of the closed clip. The in vitro immersion experiments showed that closed clips (0.118 ± 0.041 mg·cm^{-2}·day^{-1}) corroded slightly faster than open clips (0.094 ± 0.041 mg·cm^{-2}·day^{-1}). The micromorphological observations suggested that no signs of cracking appeared on the closed Mg alloy clip, indicating that the Mg alloy had excellent resistance to stress corrosion cracking in artificial plasma. Therefore, the newly developed Mg-Nd-Zn-Zr alloy clip is a promising candidate for applications with biodegradable hemostatic clips. However, the corrosion behavior of the Mg alloy hemostatic clip in vivo and effects of the corrosion products on vascular recovery need to be further studied.

Author Contributions: L.M. and C.S. conceived this project. L.M. and X.Z. (Xin Zheng) carried out the structural design and finite element simulation. L.M. and C.S. designed the experiments for material synthesis, microstructural characterizations, and degradation measurements. L.M., X.Z. (Xin Zheng), and Y.T. performed experiments, and collected and analyzed the relevant data. Y.S. and X.Z. (Xiaochen Zhang) participated in the collection and arrangement of the literature. All authors contributed to the writing of manuscript. All authors have read and agreed to the published version of the manuscript.

Funding: This work was supported by the National Natural Science Foundation of China (Grant Nos. 51901137, 51735003) and National Key R&D Program of Ministry of Science and Technology-digital medical equipment R&D (Grant No. 2019YFC0120402).

Institutional Review Board Statement: Not applicable.

Informed Consent Statement: Not applicable.

Data Availability Statement: Not applicable.

Conflicts of Interest: The authors declare no conflict of interest.

References

1. Ikeo, N.; Nakamura, R.; Naka, K.; Hashimoto, T.; Yoshida, T.; Urade, T.; Fukushima, K.; Yabuuchi, H.; Fukumoto, T.; Ku, Y.; et al. Fabrication of a magnesium alloy with excellent ductility for biodegradable clips. *Acta Biomater.* **2016**, *29*, 468–476. [CrossRef]
2. Ooi, B.P.; Hassan, M.R.; Kiew, K.K.; Chin, K.L.; Zalwani, Z. Case report of a hemostatic clip being retained for 2 years after deployment. *Gastrointest. Endosc.* **2010**, *72*, 1315–1316. [CrossRef] [PubMed]
3. Ding, P.; Liu, Y.; He, X.; Liu, D.; Chen, M. In vitro and in vivo biocompatibility of Mg–Zn–Ca alloy operative clip. *Bioact. Mater.* **2019**, *4*, 236–244. [CrossRef] [PubMed]

4. Yoshida, T.; Fukumoto, T.; Urade, T.; Kido, M.; Toyama, H.; Asari, S.; Ajiki, T.; Ikeo, N.; Mukai, T.; Ku, Y. Development of a new biodegradable operative clip made of a magnesium alloy: Evaluation of its safety and tolerability for canine cholecystectomy. *Surgery* **2017**, *161*, 1553–1560. [CrossRef]
5. Filli, L.; Luechinger, R.; Frauenfelder, T.; Beck, S.; Guggenberger, R.; Farshad-Amacker, N.; Andreisek, G. Metal-induced artifacts in computed tomography and magnetic resonance imaging: Comparison of a biodegradable magnesium alloy versus titanium and stainless steel controls. *Skelet. Radiol.* **2014**, *44*, 849–856. [CrossRef]
6. Javed, F.; Al-Hezaimi, K.; Almas, K.; Romanos, G.E. Is Titanium Sensitivity Associated with Allergic Reactions in Patients with Dental Implants? A Systematic Review. *Clin. Implant Dent. Relat. Res.* **2011**, *15*, 47–52. [CrossRef]
7. Fage, S.W.; Muris, J.; Jakobsen, S.S.; Thyssen, J.P. Titanium: A review on exposure, release, penetration, allergy, epidemiology, and clinical reactivity. *Contact Dermat.* **2016**, *74*, 323–345. [CrossRef] [PubMed]
8. Yu, X.; Li, D.; Liu, Y.; Ding, P.; He, X.; Zhao, Y.; Chen, M.; Liu, D. In vitro and in vivo studies on the degradation and biosafety of Mg-Zn-Ca-Y alloy hemostatic clip with the carotid artery of SD rat model. *Mater. Sci. Eng. C* **2020**, *115*, 111093. [CrossRef]
9. Tan, T.M.; Okada, M. The efficiency of absorbable clips in minimally invasive surgery. *Surg. Today* **1999**, *29*, 828–831. [CrossRef]
10. Mao, L.; Shen, L.; Chen, J.; Zhang, X.; Kwak, M.; Wu, Y.; Fan, R.; Zhang, L.; Pei, J.; Yuan, G.; et al. A promising biodegradable magnesium alloy suitable for clinical vascular stent application. *Sci. Rep.* **2017**, *7*, 46343. [CrossRef]
11. Abdel-Gawad, S.A.; Shoeib, M.A. Corrosion studies and microstructure of Mg−Zn−Ca alloys for biomedical applications. *Surfaces Interfaces* **2019**, *14*, 108–116. [CrossRef]
12. Zhou, H.; Liang, B.; Jiang, H.; Deng, Z.; Yu, K. Magnesium-based biomaterials as emerging agents for bone repair and regeneration: From mechanism to application. *J. Magnes. Alloys* **2021**, *9*, 779–804. [CrossRef]
13. Liu, C.; Ren, Z.; Xu, Y.; Pang, S.; Zhao, X.; Zhao, Y. Biodegradable Magnesium Alloys Developed as Bone Repair Materials: A Review. *Scanning* **2018**, *2018*, 9216314. [CrossRef]
14. Kumar, K.; Gill, R.S.; Batra, U. Challenges and opportunities for biodegradable magnesium alloy implants. *Mater. Technol.* **2017**, *33*, 153–172. [CrossRef]
15. Zhang, Y.; Li, J.; Li, J. Effects of microstructure transformation on mechanical properties, corrosion behaviors of Mg-Zn-Mn-Ca alloys in simulated body fluid. *J. Mech. Behav. Biomed. Mater.* **2018**, *80*, 246–257. [CrossRef]
16. Radha, R.; Sreekanth, D. Insight of magnesium alloys and composites for orthopedic implant applications—A review. *J. Magnes. Alloy.* **2017**, *5*, 286–312. [CrossRef]
17. Han, H.-S.; Loffredo, S.; Jun, I.; Edwards, J.; Kim, Y.-C.; Seok, H.-K.; Witte, F.; Mantovani, D.; Glyn-Jones, S. Current status and outlook on the clinical translation of biodegradable metals. *Mater. Today* **2019**, *23*, 57–71. [CrossRef]
18. Mao, L.; Shen, L.; Niu, J.; Zhang, J.; Ding, W.; Wu, Y.; Fan, R.; Yuan, G. Nanophasic biodegradation enhances the durability and biocompatibility of magnesium alloys for the next-generation vascular stents. *Nanoscale* **2013**, *5*, 9517–9522. [CrossRef]
19. Collins, M.N.; Ren, G.; Young, K.; Pina, S.; Reis, R.L.; Oliveira, J.M. Scaffold Fabrication Technologies and Structure/Function Properties in Bone Tissue Engineering. *Adv. Funct. Mater.* **2021**, *31*, 2010609. [CrossRef]
20. Ma, J.; Zhao, N.; Betts, L.; Zhu, D. Bio-Adaption between Magnesium Alloy Stent and the Blood Vessel: A Review. *J. Mater. Sci. Technol.* **2016**, *32*, 815–826. [CrossRef]
21. Sampatirao, H.; Radhakrishnapillai, S.; Dondapati, S.; Parfenov, E.; Nagumothu, R. Developments in plasma electrolytic oxidation (PEO) coatings for biodegradable magnesium alloys. *Mater. Today: Proc.* **2021**, *46*, 1407–1415. [CrossRef]
22. Song, G. Control of biodegradation of biocompatable magnesium alloys. *Corros. Sci.* **2007**, *49*, 1696–1701. [CrossRef]
23. Tian, P.; Liu, X.; Ding, C. In vitro degradation behavior and cytocompatibility of biodegradable AZ31 alloy with PEO/HT composite coating. *Colloids Surf. B Biointerfaces* **2015**, *128*, 44–54. [CrossRef] [PubMed]
24. Mao, L.; Shen, L.; Chen, J.; Wu, Y.; Kwak, M.; Lu, Y.; Xue, Q.; Pei, J.; Zhang, L.; Yuan, G.; et al. Enhanced Bioactivity of Mg–Nd–Zn–Zr Alloy Achieved with Nanoscale MgF_2 Surface for Vascular Stent Application. *ACS Appl. Mater. Interfaces* **2015**, *7*, 5320–5330. [CrossRef] [PubMed]
25. Mao, L.; Zhou, H.; Chen, L.; Niu, J.; Zhang, L.; Yuan, G.; Song, C. Enhanced biocompatibility and long-term durability in vivo of Mg-Nd-Zn-Zr alloy for vascular stent application. *J. Alloys Compd.* **2017**, *720*, 245–253. [CrossRef]
26. Zhang, X.; Yuan, G.; Mao, L.; Niu, J.; Ding, W. Biocorrosion properties of as-extruded Mg–Nd–Zn–Zr alloy compared with commercial AZ31 and WE43 alloys. *Mater. Lett.* **2012**, *66*, 209–211. [CrossRef]
27. Tan, L.; Yu, X.; Wan, P.; Yang, K. Biodegradable Materials for Bone Repairs: A Review. *J. Mater. Sci. Technol.* **2013**, *29*, 503–513. [CrossRef]
28. Li, T.; Zhang, H.; He, Y.; Wen, N.; Wang, X. Microstructure, Mechanical Properties and In Vitro Degradation Behavior of a Novel Biodegradable Mg–1.5Zn–0.6Zr–0.2Sc Alloy. *J. Mater. Sci. Technol.* **2015**, *31*, 744–750. [CrossRef]
29. Jafari, S.; Raman, R.K. In-vitro biodegradation and corrosion-assisted cracking of a coated magnesium alloy in modified-simulated body fluid. *Mater. Sci. Eng. C* **2017**, *78*, 278–287. [CrossRef]
30. Zhao, D.; Witte, F.; Lu, F.; Wang, J.; Li, J.; Qin, L. Current status on clinical applications of magnesium-based orthopaedic implants: A review from clinical translational perspective. *Biomaterials* **2017**, *112*, 287–302. [CrossRef]
31. Zhang, J.; Li, H.; Wang, W.; Huang, H.; Pei, J.; Qu, H.; Yuan, G.; Li, Y. The degradation and transport mechanism of a Mg-Nd-Zn-Zr stent in rabbit common carotid artery: A 20-month study. *Acta Biomater.* **2018**, *69*, 372–384. [CrossRef] [PubMed]
32. Tong, P.; Sheng, Y.; Hou, R.; Iqbal, M.; Chen, L.; Li, J. Recent progress on coatings of biomedical magnesium alloy. *Smart Mater. Med.* **2022**, *3*, 104–116. [CrossRef]

33. Tsakiris, V.; Tardei, C.; Clicinschi, F.M. Biodegradable Mg alloys for orthopedic implants—A review. *J. Magnes. Alloys* **2021**, *9*, 1884–1905. [CrossRef]
34. Merson, E.; Poluyanov, V.; Myagkikh, P.; Merson, D.; Vinogradov, A. Inhibiting stress corrosion cracking by removing corrosion products from the Mg-Zn-Zr alloy pre-exposed to corrosion solutions. *Acta Mater.* **2021**, *205*, 116570. [CrossRef]
35. Liu, J.; Song, Y.; Shan, D.; Han, E.-H. Different Microgalvanic Corrosion Behavior of Cast and Extruded EW75 Mg Alloys. *J. Electrochem. Soc.* **2016**, *163*, C856–C863. [CrossRef]
36. Bakhsheshi-Rad, H.R.; Abdellahi, M.; Hamzah, E.; Ismail, A.F.; Bahmanpour, M. Modelling corrosion rate of biodegradable magnesium-based alloys: The case study of Mg-Zn-RE-xCa (x = 0, 0.5, 1.5, 3 and 6 wt%) alloys. *J. Alloys Compd.* **2016**, *687*, 630–642. [CrossRef]
37. Argade, G.R.; Panigrahi, S.K.; Mishra, R.S. Effects of grain size on the corrosion resistance of wrought magnesium alloys containing neodymium. *Corros. Sci.* **2012**, *58*, 145–151. [CrossRef]
38. Atrens, A.; Song, G.-L.; Cao, F.; Shi, Z.; Bowen, P.K. Advances in Mg corrosion and research suggestions. *J. Magnes. Alloys* **2013**, *1*, 177–200. [CrossRef]
39. Tekin, K.C.; Malayoğlu, U.; Shrestha, S. Electrochemical behavior of plasma electrolytic oxide coatings on rare earth element containing Mg alloys. *Surf. Coat. Technol.* **2013**, *236*, 540–549. [CrossRef]
40. Arrabal, R.; Pardo, A.; Merino, M.; Mohedano, M.; Casajús, P.; Paucar, K.; Garcés, G. Effect of Nd on the corrosion behaviour of AM50 and AZ91D magnesium alloys in 3.5wt.% NaCl solution. *Corros. Sci.* **2012**, *55*, 301–312. [CrossRef]
41. Arrabal, R.; Mingo, B.; Pardo, A.; Matykina, E.; Mohedano, M.; Merino, M.; Rivas, A.; Maroto, A. Role of alloyed Nd in the microstructure and atmospheric corrosion of as-cast magnesium alloy AZ91. *Corros. Sci.* **2015**, *97*, 38–48. [CrossRef]
42. Gerashi, E.; Alizadeh, R.; Langdon, T.G. Effect of crystallographic texture and twinning on the corrosion behavior of Mg alloys: A review. *J. Magnes. Alloys* **2021**, *10*, 313–325. [CrossRef]
43. Aung, N.N.; Zhou, W. Effect of grain size and twins on corrosion behaviour of AZ31B magnesium alloy. *Corros. Sci.* **2010**, *52*, 589–594. [CrossRef]